Available online at www.sciencedirect.com
ScienceDirect
Trans. Nonferrous Met. Soc. China 25(2015) 429−436
Transactions of Nonferrous Metals Society of China
www.tnmsc.cn

Evaluation of dynamic performance and ballistic behavior of Ti−5Al−5Mo−5V−3Cr−1Zr alloy

Yan-ling WANG, Song-xiao HUI, Rui LIU, Wen-jun YE

State Key Laboratory for Fabrication and Processing of Nonferrous Metals,
General Research Institute for Nonferrous Metals, Beijing 100088, China

Received 11 April 2014; accepted 13 July 2014

Abstract: Terminal ballistic tests using 7.62 mm armor-piercing incendiary (API) projectiles were performed to evaluate the resistance to penetration of Ti−5Al−5Mo−5V−3Cr−1Zr (Ti-55531) alloy. The dynamic properties were determined by a split Hopkinson pressure bar (SHPB) test system. Ti-55531 plates were subjected to two kinds of heat treatments, leading to the formation of high-strength and high-toughness plates. The results of SHPB test exhibit that the maximum impact absorbed energy of the high-strength plate at a strain rate of 2200 s^{-1} is 270 MJ/m^3; however, the maximum value for the high-toughness plate at a strain rate of 4900 s^{-1} is 710 MJ/m^3. The ballistic limit velocities for the high-strength and high-toughness plates with dimensions of 300 mm×300 mm×8 mm are 330 and 390 m/s, respectively. Excellent dynamic properties of Ti-55531 alloy correspond to good resistance to penetration. The microstructure evolution related to various impact velocities are observed to investigate the failure mechanism.

Key words: Ti−5Al−5Mo−5V−3Cr−1Zr alloy; dynamic property; split Hopkinson pressure bar; adiabatic shear band; ballistic behavior; ballistic limit

1 Introduction

Light weight and cost effective titanium (Ti) and its alloys, with excellent mechanical, ballistic, and corrosion properties, are important candidates for armors. Ti−6Al−4V (Ti-64) has attracted significant attentions because of its high specific strength, excellent corrosion resistance and high mass efficiency. Till date, Ti-64 is the best available alloy for armor. Therefore, numerous studies have been carried out to reveal the ballistic behavior of Ti-64 under various conditions [1−4].

In particular, Ti-64 is susceptible to shear localization at high strain and strain rate ballistic impact or dynamic loading [5]. In the ballistic impact regime, target plugging (occurring for the flat projectiles with dimensions equal to the thickness of the targets) is a significantly distinguished example of inhomogeneous and narrow shear band formation leading to catastrophic failure [1]. MURR et al [1] investigated microstructures and microstructure evolution associated with adiabatic shear band (ASB) formation in ballistic plugging in Ti-64 targets impacted by steel projectiles. They observed that the cracks nucleated and propagated within the ASBs and the width of the ASB increased with increasing velocity. Moreover, they summarized the evolutionary sequence of ASBs and cracks. First, shear localization created dense dislocation zone, which was followed by its recrystallization in dense dislocation zone leading to the formation of ASB. Subsequently, deformation occurred followed by the nucleation, growth, and propagation of crack in ASB. Finally, coalescence and propagation of cracks resulted in a failure of the alloy.

Better understanding of the relationship between ballistic behavior and dynamic properties of Ti plates could help to deduce ballistic protection from dynamic strength or plastic strain. Therefore, ME-BAR and ROSENBERG [4] attempted to correlate the ballistic performance of differently treated Ti-64 plates with their dynamic properties. They indicated that it was not easy to make simple correlations between different sets of experiments because of the significant difference in the states of stress, although their mode of failure was both

Foundation item: Project (2012 DFG51540) supported by the Ministry of Science and Technology of China
Corresponding author: Song-xiao HUI, Tel: +86-10-82241167, E-mail: huisx@grinm.com
DOI: 10.1016/S1003-6326(15)63620-2

related to adiabatic shear hand.

The use of β and near β Ti alloys is gradually increasing for structural applications because they exhibit good workability. Ti−5Al−5Mo−5V−3Cr−1Zr (Ti-55531) is a near β alloy due to the presence of large amount of molybdenum, vanadium and chromium. The correlations between the strengths of the specimens or their impact absorbed energy and the ballistic data of differently treated Ti-55531 Ti alloy have rarely been investigated. Therefore, the objective of this work was to obtain the excellent dynamic properties of Ti-55531 corresponding to resistance to penetration. In particular, microstructure features at various impact velocities were observed in order to investigate the failure mechanisms of Ti-55531 plates.

2 Experimental

2.1 Experimental materials

The chemical composition of Ti-55531 alloy is listed in Table 1. Ti-55531 plates were subjected to two heat treatments leading to the formation of high-strength and high-toughness plates. The bars and plates used in this work were manufactured by Baotai Group, China. Bars (d15 mm × 60 mm) and thick plates (300 mm × 300 mm × 8 mm) were subjected to solution treatment and aging treatment in accordance with the classic rules of China Aeronautical Materials Handbook [6] and FU's results [7]. Specific heat treatment and the resulting mechanical properties measured using standard specimens are listed in Table 2.

2.2 Ballistic tests

Ballistic test devices are shown in Fig. 1. 53 type 7.62 mm WO-109C armor-piercing incendiary (API) projectile was selected for this work due to its appropriate test projectile in GJB 59.18—88 [8]. The test distance was 14 m and the impact velocity was varied by adjusting the mass of propellant (Δm). The ballistic limit (v_{50}) refers to the velocity of a projectile having a penetration probability of 50%. Thus, higher values of v_{50} indicate more excellent ballistic performance [2].

2.3 Split Hopkinson pressure bar experiments

Split Hopkinson pressure bar (SHPB) is recognized as a useful experimental technology to obtain constitutive model under medium strain rates in the range of 10^2 to 10^4 s^{-1} [9]. SHPB was developed and used by HOPKINSON, DAVIES, and KOLSKY [10−12]. However, an improved version of the device was employed in this work. For investigating moderate strain rate (10^2–10^4 s^{-1}), SHPB technique has been recognized universally [13].

Typical SHPB devices, and data acquisition and processing system are schematically shown in Fig. 2.

The dimensions of the specimen used in SHPB tests were d5 mm × 5 mm and d4 mm × 4 mm; however, the compression axis was parallel to the rolling direction. The specimen used in SHPB test should reach an accuracy of 0.01 mm. During SHPB experiment, the test under each strain rate should be repeated at least three times to enhance the credibility of the data and to avoid experimental scatter resulting from different specimens.

Table 1 Chemical composition of Ti-55531 titanium alloy (mass fraction, %)

Al	Mo	V	Cr	Zr	O	N	C	H	Ti
5.46	4.96	5.07	3.06	1.20	0.068	0.020	0.021	0.0010	Balance

Table 2 Mechanical properties of Ti-55531 titanium alloy after two heat treatments

Sample	Heat treatment	t_β/°C	Yield strength/MPa	Ultimate tensile strength/MPa	Elongation/%	Reduction in area/%
High-strength plate	(820 °C/1 h, AC)+(580 ℃/4 h, AC)	850	1340	1370	9.0	23
High-toughness plate	(820 °C/1 h, FC)+(610 °C /4 h, AC)		1035	1100	19	53

AC: Air cooled; FC: Furnace cooled

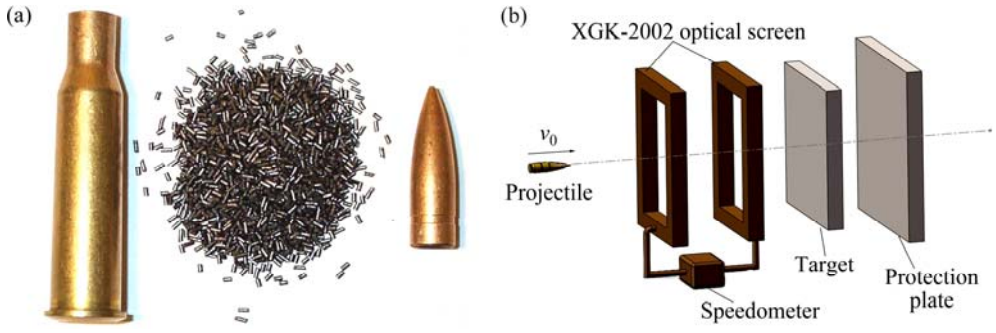

Fig. 1 Schematic diagram of ballistic test devices: (a) Projectiles; (b) Test system

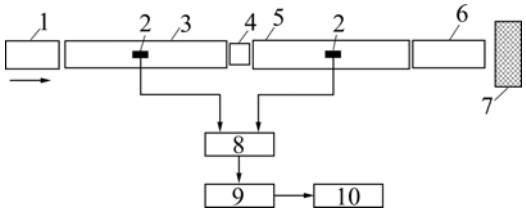

Fig. 2 Schematic illustration of Hopkinson pressure bar system: 1—Trip lever; 2—Strain gauge sensor; 3—Incident bar; 4—Specimen; 5—Transmission rod; 6—Damping rod; 7—Damper; 8—Super dynamic strain apparatus; 9—Transient waveform memory; 10—Data processing system

For optical microscopy analysis, the bullet holes of ballistic test were sectioned in half along the penetration direction and the recovered specimens of SHPB test were cut along the compression axis before pre-grinding and electrolytic polishing, performed according to the standard metallographic preparation procedures. The etching was performed in Kroll's solution (V(HF): $V(HNO_3)$:$V(H_2O)$=1:3:7) to reveal the microstructure. The microstructure was observed by Axiovert-200 MAT optical microscope (OM).

3 Results and discussion

3.1 Ballistic efficiency

The original records of piercing experiments are listed in Tables 3 and 4. The values of v_{50} for high-strength and high-toughness plates are 330 and 390 m/s, respectively. In this work, when a target is impacted by a projectile, partial or complete penetration is achieved. A complete penetration occurs when a piece of target or

Table 3 Firing data for 7.62 mm API vs high-strength plate at 0° obliquity (v_{50}=330 m/s)

Shot No.	Δm/g	v_0/ (m·s^{-1})	Comment
101	1.50	404	Invalid
102	1.50	431	Complete penetration
103	1.40	367	Complete penetration
104	1.35	358	Complete penetration
105	1.30	355	Partial penetration, back cracks
106	1.30	360	Partial penetration, back cracks
107	1.25	337	Complete penetration
108	1.25	361	Complete penetration
109	1.20	334	Invalid
110	1.20	334	Partial penetration, bulge, small cracks
111	1.20	339	Partial penetration, bulge, small cracks
112	1.15	321	Partial penetration, bulge, small cracks
113	1.15	320	Partial penetration, bulge, small cracks

Table 4 Firing data for 7.62 mm API vs high-toughness plate at 0° obliquity (v_{50}=390 m/s)

Shot No.	Δm/g	v_0/ (m·s^{-1})	Comments
201	1.50	410	Complete penetration
202	1.50	400	Complete penetration
203	1.50	389	Partial penetration, back cracks
204	1.40	371	Partial penetration, bulge, small cracks
205	1.35	361	Partial penetration
206	1.35	360	Partial penetration, bulge, small cracks
207	1.32	359	Partial penetration, bulge, small cracks
208	1.28	363	Partial penetration, bulge, small cracks
209	1.25	343	Partial penetration, bulge
210	1.50	413	Complete penetration

penetrator material perforates the rear screen; however, all other impact cases result in partial penetration.

Low-magnification images of the penetration channel of high-toughness and high-strength plates are shown in Fig. 3. An increase in the penetration velocity of projectiles aggravates the degree of damage of high-toughness and high-strength plates, caused by the projectiles. When the high-toughness plate is impacted at a penetration velocity of v_0=360 m/s, the target board is not penetrated, and the bulging shows rifts. API penetrates into the armor to a depth of approximately 0.8H (H is the thickness of plate). However, when the penetration velocity is increased to v_0=400 m/s, the penetration hole of the target board is damaged, and the bullet fails to penetrate the target board. Moreover, a block is extruded from the front side of the target board with the appearance of a 0.3H of bulging combined with spalling at the back side of the target board. The edge of the hole made by bullet displays cracks. In contrast, when the high-strength plate is impacted at a penetration velocity of v_0=367 m/s, the target board displays higher degree of damage, and slight bulging appears along with the appearance of large crack at the back side of the target board. Moreover, the edge of bullet hole show cracks and delamination; however, its bottom does not exhibit spalling. When the high-strength plate is impacted at a penetration velocity of v_0=431 m/s, the target board is penetrated by the bullet and damaged by a typical plugging technique. The size of bullet hole at the bullet exit is 1.7 times larger than that at the entry. When the fragile or heavy plate is struck by the projectile, damage by the plugging mechanism is the most vulnerable [14].

The local OM image of Fig. 3(a) is shown in Fig. 4 which reveals cracks and ASB around the bullet hole. Figure 4(b) displays the trend and clear picture of

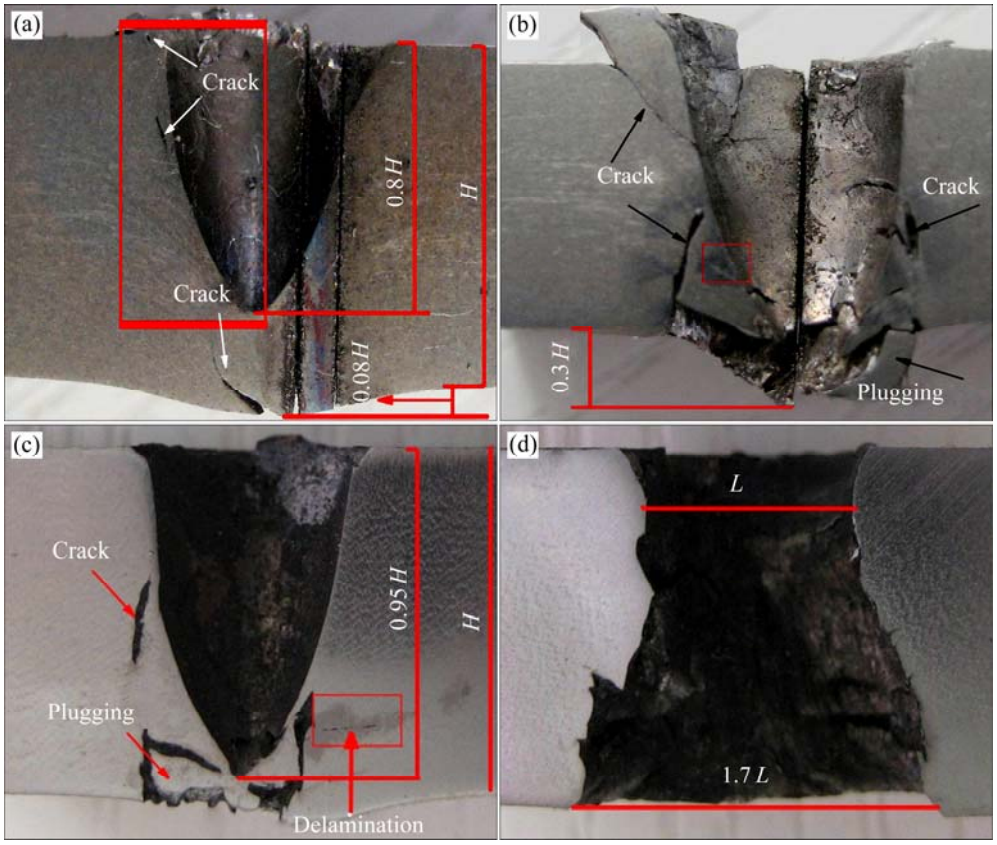

Fig. 3 Low-magnification images of penetration channel: (a) High-toughness plate, v_0=360 m/s, shot No. 206; (b) High-toughness plate, v_0=400 m/s, shot No. 202; (c) High-strength plate, v_0=367 m/s, shot No. 103; (d) High-strength plate, v_0=431 m/s, shot No. 102

the morphology of ASB. It shows that the crack expands along ASB as described in Ref. [15]. The shear band shows bifurcation during its propagation process. In general, the bifurcated secondary shear band is narrower, which gradually disappears during the propagation process. At the bottom of the bullet hole, an approximate arc-shaped ASB with a width of 1–5 μm is obtained between the arc-shaped bullet hole and the matrix structure, along with irregular bifurcation. The cracks around the arc-shaped ASB wrapped at the bottom of the bullet hole are not observed.

Two distinctive ASB morphologies are observed in the structure: the first is the dark band in Zone *A*, and the second is the white and bright band in Zone *B* as shown in Fig. 4(b). The enlarged microstructure within Zone *A* (Fig. 4(c)) exhibits that the width of the dark band is 1–8 μm, indicating an obvious border line with the matrix structure. Therefore, the structure within the band is difficult to be distinguished clearly under OM. Furthermore, the enlarged structural image within Zone *B* (Fig. 4(d)) reveals that the width of the bright band is about 20 μm, including the central band and transition band. The structures within the central band and transition band cannot be clearly observed under OM. Figure 4 reveals that the bright band and the matrix structure are connected by the transition band, and the border line between the two bands is not as distinct as that between the dark band and the matrix structure.

LI et al [16] studied the shear band formation in impacted Ti-64 and observed the following two types of ASB bands: deformed and white-etching bands. The deformed bands formed at the initial stage and further studies [17,18] revealed that the white-etching bands developed within the deformed bands. Moreover, the strain rate curve showed an abrupt increase corresponding to the occurrence of ASB [17,18]. Microstructural observations by transmission electron microscopy (TEM) reveal that ASB region consists of fine recrystallized equiaxed grains (0.2 μm), in contrast to the initial microstructure exhibiting a grain size of approximately 72 μm [19,20].

The investigation on the microstructure of the alloy target board demonstrates that the target board absorbs the bullet energy mainly through plastic deformation, bulging, cracks, and ASB when the high-toughness plate is impacted at the penetration velocity of 360 m/s. However, when the velocity of bullet penetrating the high-toughness plate reaches 400 m/s, fragments obtained after spalling of the target board also absorb

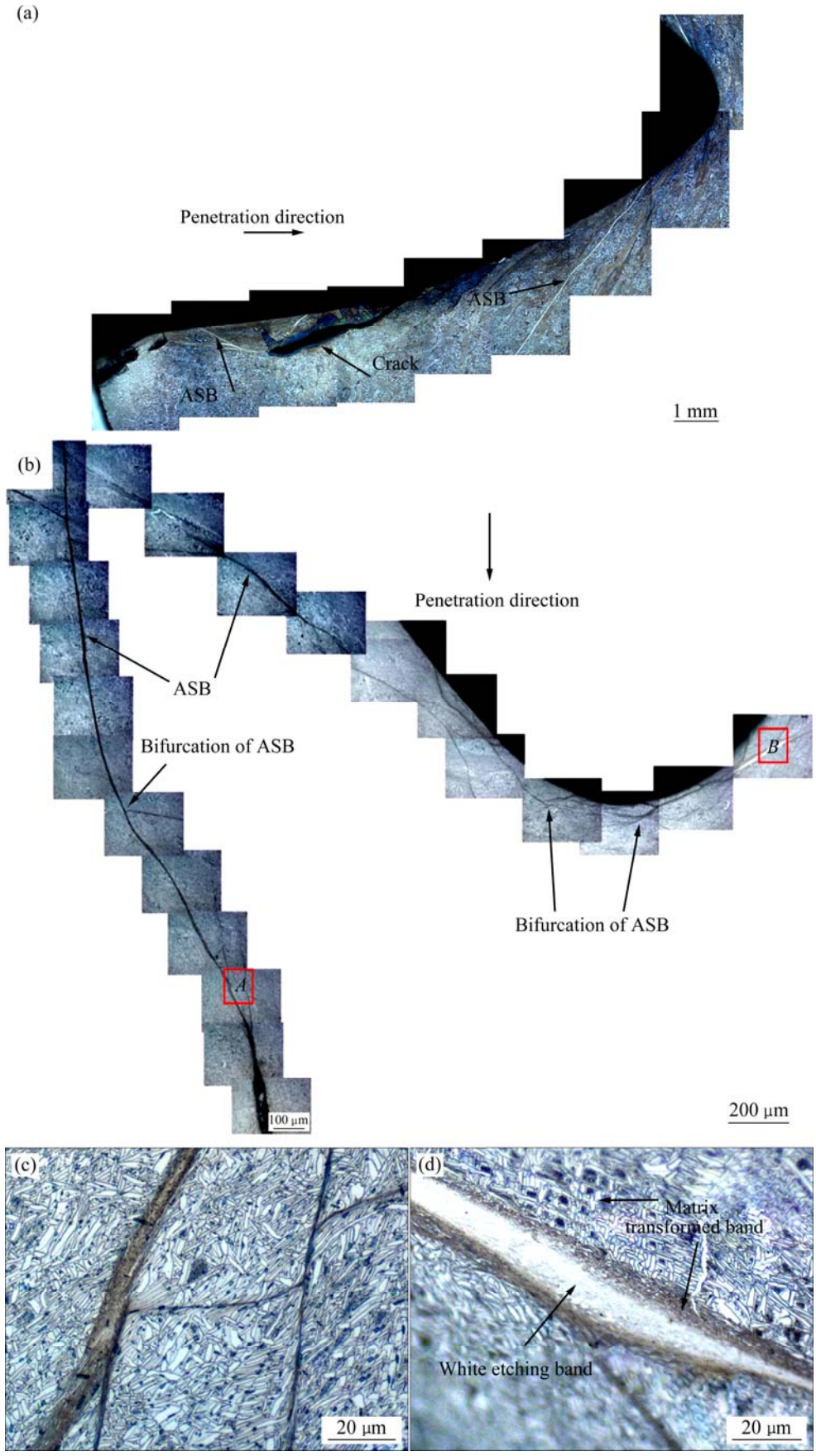

Fig. 4 Morphology and microstructure of high-toughness plates impacted at v_0=360 m/s: (a, b) OM images; (c) Enlarged image of Zone *A*; (d) Enlarged image of Zone *B*

some bullet energy, besides the energy absorption modes at a low penetration velocity.

Figure 5(a) shows the microstructure of the bullet hole exhibiting delamination and numerous microcracks around the bullet hole. The detailed features of microcracks are shown in Fig. 5(b), revealing the absence of ASB between the two microcracks. Therefore, the microstructure of the alloy target board reveals the following results: when the high-strength plate is impacted at a penetration velocity of 367 m/s, the target board absorbs the bullet energy mainly by generating cracks, microcracks, and delamination. However, when the velocity of bullet penetrating the high-strength plate reaches 431 m/s, the failure mode of the target board is transformed into plugging damage. Thus, the high strength plates fail due to the process of plugging.

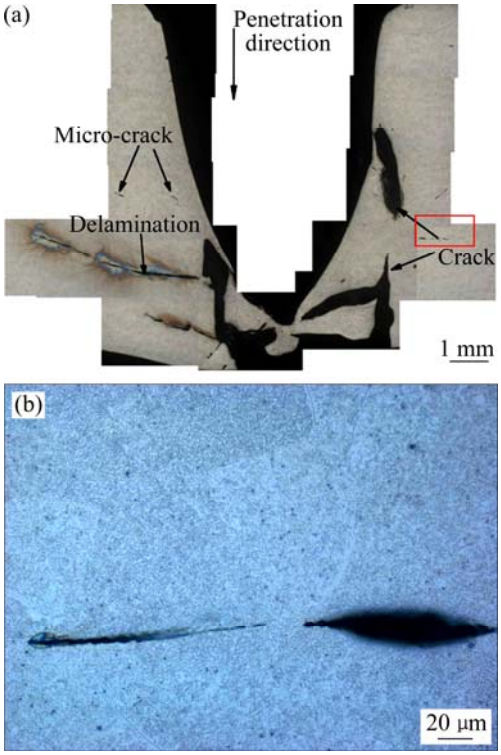

Fig. 5 Morphology and microstructure of high-strength plates impacted at v_0=367 m/s: (a) OM image; (b) Enlarged image of micro-crack

3.2 Dynamic properties

Figure 6 shows the actual stress–strain curves of the high-strength plate and high-toughness plate under the loading conditions at various strain rates. The strength and weakness of the dynamic stress–strain behavior of the material are represented by the evaluation index illustrated in Ref. [21]. The high-strength plate displays fracture failure under a strain rate of 2800 s^{-1} loading condition; the average flow stress (σ) is 1720 MPa under such a strain rate, with the homogeneous dynamic plastic strain (ε) of 0.14 and impact-absorbing energy (E) of

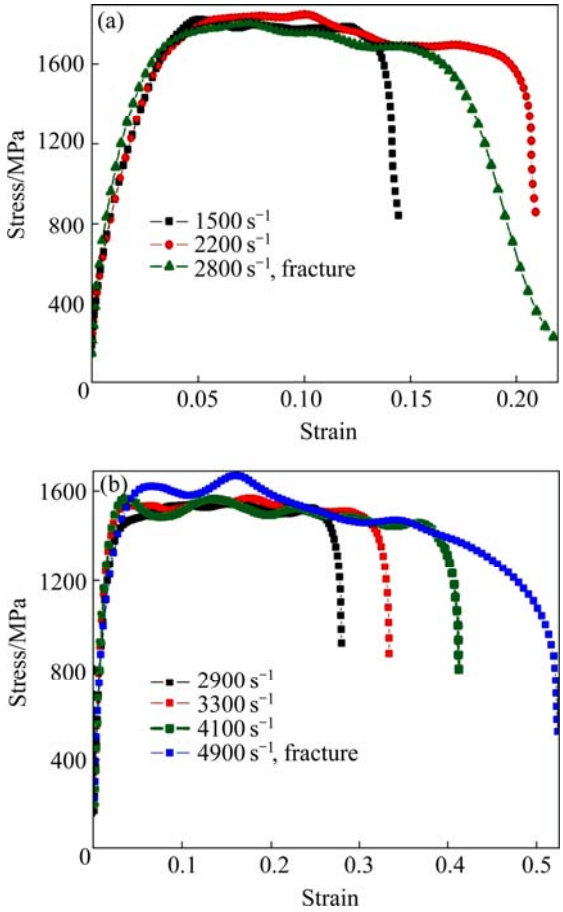

Fig. 6 Stress−strain curves of Ti-55531 alloy at various strain rates: (a) High-strength plate; (b) High-toughness plate

240 MJ/m^3. The high-toughness plate remains intact under a strain rate of 4100 s^{-1} loading condition; however, it exhibits fracture failure under a strain rate of 4900 s^{-1} loading condition.

The flow stress of the two types of plates is not sensitive to strain rate from 1500 to 4900 s^{-1}. However, a significant increase in the flow stress is observed when the strain rates are higher than 1000 s^{-1}. Thus, the above mentioned phenomenon indicates a change from a thermally-activated control of dislocation movements at low strain rates to a viscous drag control mechanism at higher strain rates [22]. In contrast, FOLLANSBEE and KOCKS [23] investigated the copper alloy, indicating that the higher flow stress is not caused by the transformation of the deformation mechanism; however, an enhanced rate of dislocation generation is responsible for the high flow stress.

The two types of plates express slight thermal softening effect with the increase in the strain rate, which is attributed to the presence of large amount of β phase with body-centered cubic (BCC) structure. Slip systems of the BCC structure play an important role in high strain rates deformation. Plugging of dislocation of BCC structure is not significant, resulting in an insignificant

effect of work hardening; however, thermal softening outweighs the effects of strain rate hardening and strain hardening in the deforming region.

The average flow stress, homogeneous dynamic plastic strain, and impact-absorbing energy of the two types of plates are calculated based on the actual stress–strain curves, as listed in Table 5. The dynamic properties of the high-toughness plate were superior compared to those of the high-strength plate.

Table 5 Average flow stress, homogeneous dynamic plastic strain, and impact-absorbing energy of Ti-55531 alloy

Sample	σ/MPa	ε	E/(MJ·m^{-3})	$\dot{\varepsilon}$ /s^{-1}	Remarks
High-strength plate	1780	0.16	270	2200	Integrity
High-toughness plate	1500	0.49	710	4900	Fracture

Figure 7 shows the microstructures of the two types of plates. The microstructure of high-strength plate consists of acicular primary α phase (α_P) and β transformation (β_T) tissues. However, the microstructure of the high-toughness plate consists of lath and equiaxed α_p and β_T tissues.

The lathed or equiaxed α_P is thicker and bigger than acicular α_P, because the high-toughness plate after solid-solution treatment adopts the way of furnace cooling, thus providing α_P with longer time to elongate and thicken at a lower cooling rate. The thickened α_P displays a superior coordinating capacity than acicular α_P

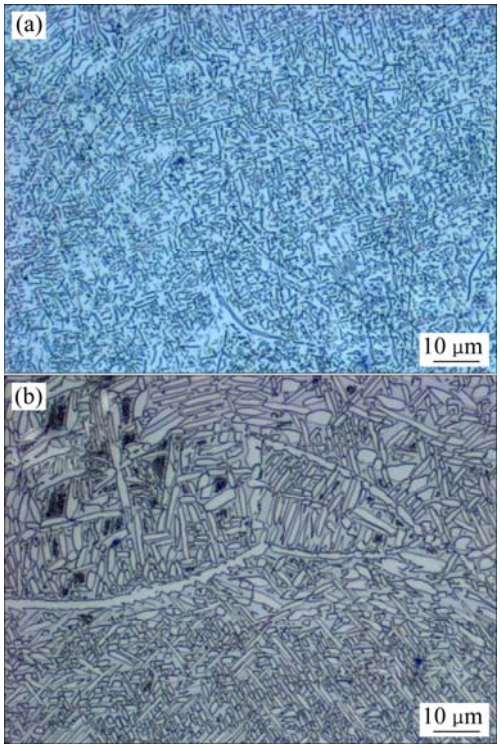

Fig. 7 Microstructures of two types of plate: (a) High-strength plate; (b) High-toughness plate

in deformation, thus causing a decrease in strength and increase in plasticity of the alloy. Good plasticity of the high-toughness plate could endow the alloy with superior dynamic and bullet-proof property.

4 Conclusions

1) The Ti-55531 alloy is subjected to two heat treatments to obtain high-strength and high-toughness plates. Importantly, the v_{50} for high-strength and high-toughness plates with dimensions of 300 mm × 300 mm × 8 mm are 330 m/s and 390 m/s, respectively. The high-strength plates fail due to the process of plugging which is a low-energy failure mode when the projectile velocity is 431 m/s. In contrast, the high-toughness plates fail by a mixed process of bulging, shearing, cracks, and spalling as the projectile velocity is 400 m/s.

2) ASBs exhibit two types of morphologies during the ballistic test of high-toughness plates, namely, deformed bands and white-etching bands.

3) The results of SHPB test show that the maximum impact absorbed energy of the high-strength plate at a strain rate of 2200 s^{-1} is 270 MJ/m^3; however, the maximum value for high-toughness plate at a strain rate of 4900 s^{-1} is 710 MJ/m^3. In this work, excellent dynamic properties of Ti-55531 alloy corresponding to good resistance to penetration are observed.

Acknowledgements

The authors wish to thank Yu REN et al of Beijing Institute of Technology for their help in carrying out SHPB tests.

References

[1] MURR L E, RAMIRESZ A C, GAYTAN S M, LOPEZ M I, MARTINEZ E Y, HERNANDEZ D H, MARTINEZ E. Microstructure evolution associated with adiabatic shear bands and shear band failure in ballistic plug formation in Ti−6Al−4V targers [J]. Mater Sci Eng A, 2009, 516(1−2): 205−216.

[2] LEE D G, LEE Y H, LEE S, LEE C S, HUR S M. Dynamic deformation behavior and ballistic impact properties of Ti−6Al−4V alloy having equiaxed and bimodal microstructures [J]. Metall Mater Trans A, 2004, 35(10): 3103−3112.

[3] BRUCHEY W J. Suppression of material failure modes in titanium armors [R]. USA: US Army Research Laboratory, 2003.

[4] ME-BAR Y, ROSENBERG Z. On the correlation between the ballistic behavior and dynamic properties of titanium-alloy plates [J]. Inter J Impact Eng, 1997, 19(4): 311−318.

[5] ZHANG Jing, TAN Cheng-wen, REN Yu, YU Xiao-dong, MA Hong-lei, WANG Fu-chi, CAI Hong-nian. Adiabatic shear fracture in Ti6Al4V alloy [J]. Transactions of Nonferrous Metals Society of China, 2011, 21(11): 2396−2401.

[6] Editorial Committee of China Aeronautical Materials Handbook. China Aeronautical Materials Handbook [M]. Beijing: China Standard Press, 2002. (in Chinese)

[7] FU Yan-yan. Research on high strength and high toughness Ti−5Al−5Mo−5V−3Cr series alloys [D]. Beijing: General Reasearch Institute for Nonferrous Metals, 2008. (in Chinese)
[8] GJB 59.18—88. Test operations procedure for armoured vehicles and armour plate bullet-proof test [S]. (in Chinese)
[9] MEYERS M A. Dynamic behavior of materials [M]. Beijing: National Defence Industry Press, 2006: 206−223.
[10] KOLSKY H. An investigation of the mechanical properties of materials at very high rates of loading [J]. Proceedings of the Physical Society B, 1949, 62(11): 676−700.
[11] HOPKINSON B. A method of measuring the pressure produced in the detonation of high explosives or by the impact of bullets [J]. Philosophical Transactions of the Royal Society A, 1914, 213(1): 437−456.
[12] DAVIES R M. A critical study of Hopkinson pressure bar [J]. Philosophical Transactions of the Royal Society A, 1948, 240(1): 375−457.
[13] FIELD J E, WALLEY S M, PROUD W G, GOLDREIN H T, SIVIOUR C R. Review of experimental techniques for high rate deformation and shock studies [J]. Inter J Impact Eng, 2004, 30(7): 725−775.
[14] QIAN Wei-chang. Mechanics of armour-piercing [M]. Beijing: National Defence Industry Press, 1984: 7−30. (in Chinese)
[15] REN Yu, TAN Cheng-wen, ZHANG Jing, WANG Fu-chi. Dynamic fracture of Ti-6Al-4V alloy in Taylor impact test [J]. Transactions of Nonferrous Metals Society of China, 2011, 21(2): 223−235.
[16] LI Q, XU Y B, LAI Z H, SHEN L T, BAI Y L. Dynamic recrystallization induced by plastic deformation at high strain rate in a Monel alloy [J]. Mater Sci Eng A, 2000, 276(1−2): 250−256.
[17] XU Y B, ZHANG J H, BAI Y L, MEYERS M A. Shear localization in dynamic deformation: Microstructural evolution [J]. Metall Mater Trans A, 2008, 39A(4): 811−834.
[18] XU Y B, ZHONG W L, CHEN Y J, SHEN L T, LIU Q, BAI Y L, MEYERS M A. Shear localization and recrystallization in dynamic deformation of 8090 Al−Li alloy [J]. Mater Sci Eng A, 2001, 299(1−2): 287−295.
[19] YANG Y, JIANG F, ZHOU B M, LI X M, ZHENG H G, ZHANG Q M. Microstructural characterization and evolution mechanism of adiabatic shear band in a near beta-Ti alloy [J]. Mater Sci Eng A, 2011, 528(6): 2787−2794.
[20] MEYERS M A, SUBHASH G, KAD B K, PRASAD L. Evolution of microstructure and shear-band formation in α-hcp titanium [J]. Mechanics of Mater, 1994, 17(2−3): 175−193.
[21] LIU Qing-hua, HUI Song-xiao, YE Wen-jun, WANG Guo, HU Guang-shan. Effect of primary α phase content on dynamic stress-strain behavior of TC4ELI titanium alloy [J]. The Chinese Journal of Nonferrous Metals, 2012, 22(10): 2749−2755. (in Chinese)
[22] LEE W S, LIN C F CHEN T H, HWANG H H. Effects of strain rate and temperature on mechanical behaviour of Ti-15 Mo-5 Zr-3 Al alloy [J]. J Mech Behav Biomed Mater, 2008, 1(4): 336−344.
[23] FOLLANSBEE P S, KOCKS U F. A constitutive description of the deformation of copper based on the use of the mechanical threshold stress as an internal state variable [J]. Acta Materialia, 1988, 36(1): 81−93.

Ti−5Al−5Mo−5V−3Cr−1Zr 钛合金动态性能与弹道行为

王艳玲，惠松骁，刘 睿，叶文君

北京有色金属研究总院 有色金属材料制备加工国家重点实验室，北京 100088

摘 要：通过抗 7.62 mm 口径穿甲燃烧弹试验评估 Ti−5Al−5Mo−5V−3Cr−1Zr(Ti-55531)合金抗弹行为，采用分离式霍普金森压杆试验(SHPB)研究合金动态性能。Ti-55531 钛合金板通过 2 种热处理制度得到高强板和高韧板。SHPB 试验结果表明：高强板在 2200 s^{-1} 应变速率加载条件下，最大冲击吸收功为 270 MJ/m^3；高韧板在 4900 s^{-1} 应变速率加载条件下，最大冲击吸收功为 710 MJ/m^3。8 mm 厚高强板和高韧板的弹道极限速度分别为 330 m/s 和 390 m/ s。本实验条件下，Ti-55531 合金良好的动态性能导致其具有优异的抗弹性能。通过不同侵彻速度下组织演化探讨了合金板的失效机制。

关键词：Ti−5Al−5Mo−5V−3Cr−1Zr 合金；动态性能；霍普金森压杆；绝热剪切带；弹道行为；弹道极限

(Edited by Yun-bin HE)